Polymer Chemistry

ROYAL SOCIETY OF CHEMISTRY

PAPER

View Article Online
View Journal | View Issue

Cite this: *Polym. Chem.*, 2025, **16**, 963

Frontal polymerization of thiol–acrylate covalent adaptable networks†

Christoph Schmidleitner, [a,b] Matthias Udo Kriehuber,[a] Roman Korotkov,[a] Sandra Schlögl *[a] and Elisabeth Rossegger *[a,b]

Frontal polymerization is a curing method that is known for its high conversion, short reaction times and low energy consumption. However, the resulting materials are typical thermosets, allowing no reprocessing, reshaping nor recycling. Herein, a new approach is pursued, which combines the energy efficiency of frontal polymerization with the unique post-processability of covalent adaptable networks. Thus, selected thiol–acrylate resins, bearing a sufficiently high number of ester linkages and free hydroxyl groups, were investigated, using phosphate esters as transesterification catalysts. The amount of phosphate ester and thiol was varied and its influence on material properties and frontal polymerization kinetics was analyzed. The reaction kinetics were studied with FTIR and photo-DSC measurements, showing a trend towards lower reactivity and higher conversions with an increased thiol content. The obtained networks exhibited tunable bond exchange rates by varying either the amount of thiol or of the catalyst. DMA measurements revealed a higher network homogeneity with increasing thiol content. Moreover, reprocessing, recycling as well as reshaping of the material were successfully demonstrated. To conclude, these findings could significantly lower energy consumption and increase circularity in future thermoset production.

Received 4th October 2024,
Accepted 2nd January 2025

DOI: 10.1039/d4py01106f

rsc.li/polymers

1. Introduction

Frontal polymerizations describe autocatalyzed reactions in which a spatially confined reaction zone propagates in a wave-like manner throughout the monomers. Autocatalysis occurs due to the exothermicity of the polymerization reaction and spreads through the monomers by thermal diffusion. To induce the chain reaction, an external trigger, such as heat or light, has to be applied. Once started, the chain reaction is only terminated when either the entire monomers are consumed or due to heat loss.[1]

Frontal polymerization has been pioneered by Pojman in 1991 when he succeeded in initiating the first reported front under ambient conditions by following a free radical curing of acrylates.[2] To date, additional polymerization types are available for frontal polymerization. One mechanism relies on radically induced cationic frontal polymerization, in which epoxides and Crivello salts in combination with a thermal radical initiator are commonly employed.[3] Recently, redox cationic frontal polymerization was introduced, which exploits a reaction between a reducing agent and an iodonium salt to prevent foaming and decomposition of the material.[4] Another reliable option is ring opening metathesis polymerization, which has been applied for the efficient curing and 3D printing of fiber reinforced polymer composites.[5]

Over the past few years, frontal polymerization has gained increased attention as a fast curing technique as in view of the ongoing energy crisis and an impending green revolution, energy efficiency has become a decisive factor in most production processes. In the conventional manufacturing of thermosets, energy-intensive curing processes have to be employed. High temperatures for elongated time periods are needed[6] and large objects such as airplane or car parts are dimensionally challenging and require large ovens to cure.[7] As an example, estimations on epoxy carbon fibre composites for a Boeing's 787 fuselage section show that the energy required for 8 h of curing in an industrial autoclave requires 350 GJ resulting in 80 tons of CO_2.[8] If this polymerization is conducted frontally, a small energy input would be sufficient. Furthermore, polymerization times can be reduced significantly from hours in an autoclave to mere minutes.[9] Generally, light induced curing can only be achieved in thin layers, otherwise the penetration depth of the incident light is too low. This problem can also be overcome by frontal polymerization.[10] As the reaction is self-catalysed, absorption does not

[a]*Polymer Competence Center Leoben GmbH (PCCL), Sauraugasse 1, 8700 Leoben, Austria. E-mail: elisabeth.rossegger@pccl.at, sandra.schloegl@pccl.at*
[b]*Graz University of Technology, Institute of Chemistry and Technology of Materials, Stremayrgasse 9, 8010 Graz, Austria*

† Electronic supplementary information (ESI) available. See DOI: https://doi.org/10.1039/d4py01106f

inhibit the curing of deeper layers. Thus, thicker samples can be cured by light induced frontal polymerization than by conventional curing.[11] Besides, frontally polymerized materials exhibit higher polymerization rates as well as shorter reaction times due to the high temperatures reached during the exothermic polymerization reaction.[12] Consequently, materials obtained by frontal polymerization are characterized by comparable and sometimes even superior mechanical properties to conventional thermosets.[13]

However, thermosets are insoluble and infusible and therefore rarely recycled. The recycling problem with this material class is steadily increasing as the amount of thermosets produced reached 44 million tons in 2022 and is since growing.[14] Of all plastics produced, only 10% were recycled in 2016.[15] As a consequence, thermoset products end up in landfills, pollute the oceans or are thermally combusted, causing even more environmental pollution.[16] These obstacles can be overcome by using covalent adaptable networks (CANs), also termed vitrimers.[17] The name covalent adaptable networks was first introduced by Bowman *et al.*[18] and describes highly cross-linked three-dimensional networks, similar to thermosets, which can undergo dynamic exchange reactions at elevated temperatures. In terms of associative CANs, the topology freezing temperature (T_v) determines the flow characteristics of the dynamic polymer networks. Below this temperature, CANs behave like classic thermosets, as the exchange reactions are very slow. However, above the T_v, the exchange reactions are activated and the material behaves like a viscoelastic fluid and can be welded, recycled or reshaped.[19]

Several types of reversible reactions can be used to prepare CANs. One of the most widely researched systems is based on transesterification reactions, as various monomers, bearing ester linkages and free hydroxyl groups, and catalysts are readily available. In this reaction, an ester linkage is associatively exchanged with an available hydroxy group in the presence of a Brønsted acid,[20] organo-metallic complexes[21] or organic bases[22] as the catalyst. Examples are CANs based on polyesters,[23] thiol–epoxide,[24] thiol–ene,[25] thiol–acrylate[26] or acrylate homo-polymerization.[27]

Combining the efficiency of frontal polymerization (see Fig. 1a) with the recyclability and reprocessability of covalent adaptable networks is a crucial imperative for large-scale energy savings in manufacturing processes and for reducing the environmental impact of thermosets. Therefore, in this work, we combine the advantages of both approaches by frontally polymerizing thiol and acrylate monomers with ester linkages and free hydroxyl groups. By radical-mediated thiol–acrylate click chemistry, dynamic photopolymers are formed,

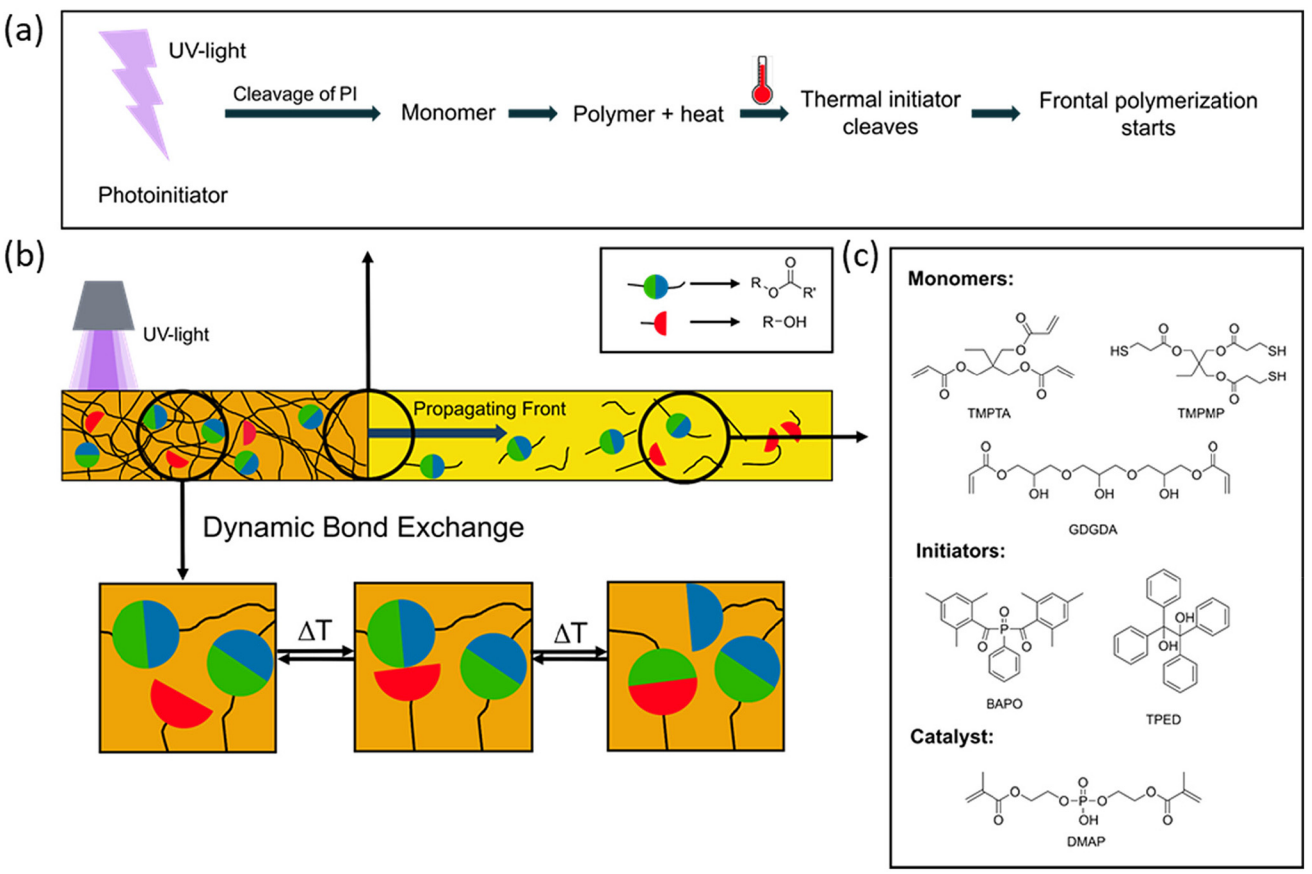

Fig. 1 (a) Scheme of frontal polymerization, (b) general overview of the frontal polymerization process and dynamic bond exchange reactions in the frontally cured photopolymers and (c) structure of the used chemicals.

which are able to undergo transesterification reactions (see Fig. 1b and c). Thiol–acrylate systems enable a convenient fine tuning of the resulting properties of the network by variation of the thiol content. A higher thiol content results in a lower glass transition temperature (T_g) and higher flexibility of the resulting photopolymer. However, it decreases the reactivity of the system and consequently the frontal velocity as well as the heat release during frontal polymerization. By finding a good balance between material properties and reactivity, photopolymers with the unique features of dynamic polymer networks were prepared. This paves the way towards the efficient production of circular photopolymer networks.

2. Results and discussion

2.1. Curing kinetics

The thiol trimethylolpropane tris(3-mercaptopropionate) (**TMPMP**) and acrylate monomers used (see Fig. 1b) allow a frontal polymerization *via* radical-mediated thiol–acrylate click chemistry and offer ample hydroxy and ester moieties for thermo-activated bond exchange reactions *via* transesterification. While the trifunctional acrylate trimethylolpropane triacrylate (**TMPTA**) was added owing to its high reactivity, the bifunctional glycerol 1,3-diglycerolate diacrylate (**GDGDA**) introduced free hydroxyl groups to the system. As a transesterification catalyst, the bifunctional phosphate ester bis[2-methacryloyloxyethyl] phosphate (**DMAP**) was applied. To enable light induced frontal polymerization, phenylbis(2,4,6-trimethylbenzoyl)phosphine oxide (**BAPO**) was used as a photoinitiator, whereas the thermal radical initiator 1,1,2,2-tetraphenyl-1,2-ethanediol (**TPED**) sustained the polymerization front.

From the literature, it is well known that frontal polymerization of pure thiol–ene systems is not working due to insufficient reaction exothermicity.[28] Thus, thiol–acrylate resins were developed herein to combine the high exothermicity of acrylate homopolymerization with the excellent homogeneity of thiol–ene step growth. In the first step, the thiol content was varied to find an optimum concentration of TMPMP (composition of the resins is summarized in Table 1 ESI†). An IR-camera was used to investigate the characteristic parameters in frontal polymerization: the maximum temperature and the front velocity. The values are listed in Table 2 ESI,† and the corresponding front propagation is depicted in Fig. 2a and c. It can be seen that with increasing thiol content, the maximum released temperature decreases from 218 ± 13 °C for SH15 to 172 ± 4 °C for SH25 and the front velocity decreases from 2.81 ± 0.06 to 1.63 ± 0.06 cm min^{-1}, respectively. In comparison, the reference sample without thiol reaches a temperature of 239 ± 11 °C and a velocity of 4.01 ± 0.22 cm min^{-1}. In contrast to expectations, this pure acrylate system reaches only slightly higher temperatures and velocities than resin SH15 and resin PH15. This is most likely due to oxygen inhibition, to which the resin is susceptible, confirming the advantage of adding thiol to the material to prevent oxygen inhibition. The trend towards decreased reactivity with an increasing amount of thiol can be attributed to two different facts. Firstly, by increasing the amount of thiol, the relative number of available carbon double bonds, which are more reactive species, is decreased per volume fraction. Secondly, these results suggest that the main driving force in frontal polymerization of thiol–acrylate resins is the high exothermicity of acrylate homopolymerization, following a chain-growth mechanism. An increased amount of thiol leads to a higher portion of thiol–ene step-growth polymerization, which reduces the overall reaction's exothermicity and slows down the frontal polymerization. A similar trend was reported in the literature, which also demonstrates a loss of reactivity for high thiol contents.[28] Moreover, a higher thiol content leads to an improved sample surface quality due to the higher amount of step growth and resulting lower temperature as well as velocity (Fig. 2b). This trend was further confirmed by photo-DSC experiments where a decrease in reaction enthalpy from 342 to 242 J g^{-1} with an increase in thiol content was observed (Fig. 2 ESI†).

Along with the thiol content, the concentration of the transesterification catalyst (organic phosphate ester) was varied to study its influence on frontal polymerization kinetics. Resins PH20 and PH25 show only a slight variation in the released temperature, which amounted to 208 ± 4 and 207 ± 3 °C, respectively (Fig. 2c). With regard to their velocity, similar values of 2.00 ± 0.08 for PH20 and 2.04 ± 0.04 cm min^{-1} for PH25 were obtained. However, a lower velocity can be expected as the measurement of temperature is more exact than the measurement of velocity. Additionally, photo-DSC measurements were performed for resins with a varying phosphate ester content. However, owing to the high reactivity of the resins, no significant differences could be detected.

To investigate the reaction kinetics and final carbon double bond conversions in more detail, FT-IR-spectroscopy measurements were carried out. The double bond conversion was calculated from the integrals of the stretching vibration of the C=C bonds at 1600–1650 cm^{-1} normalized by the carbonyl peak at 1700–1800 cm^{-1}. The resulting diagrams are depicted in Fig. 2d; the maximum conversions reached are summarized in Table 3 ESI.† By comparing resins with varying thiol content, it can be observed that formulations with a higher thiol content display higher conversions. While resin SH15 only shows 83.3% of conversion, resin SH25 features a carbon double bond conversion of 95.1%. A similar trend was reported in the literature[29] and can be attributed to the insensitivity of the thiyl radicals towards oxygen inhibition and a decrease in diffusion limitation during the reaction.

With varying phosphate ester concentrations, it was found that formulations with a higher phosphate ester content are prone to lower carbon double bond conversions. Resin PH15 shows a conversion of 84.3%, whereas resins PH20 and PH25 display 74.1% and 68.5%, respectively. A higher amount of methacrylate groups in the formulation leads to lower conversion rates as the reactivity of methacrylates is lower in the thiol–ene reaction[30] as well as in homo-polymerization.[31] However, all final conversions reached are in accordance with the literature where conversions of around 80% were reported

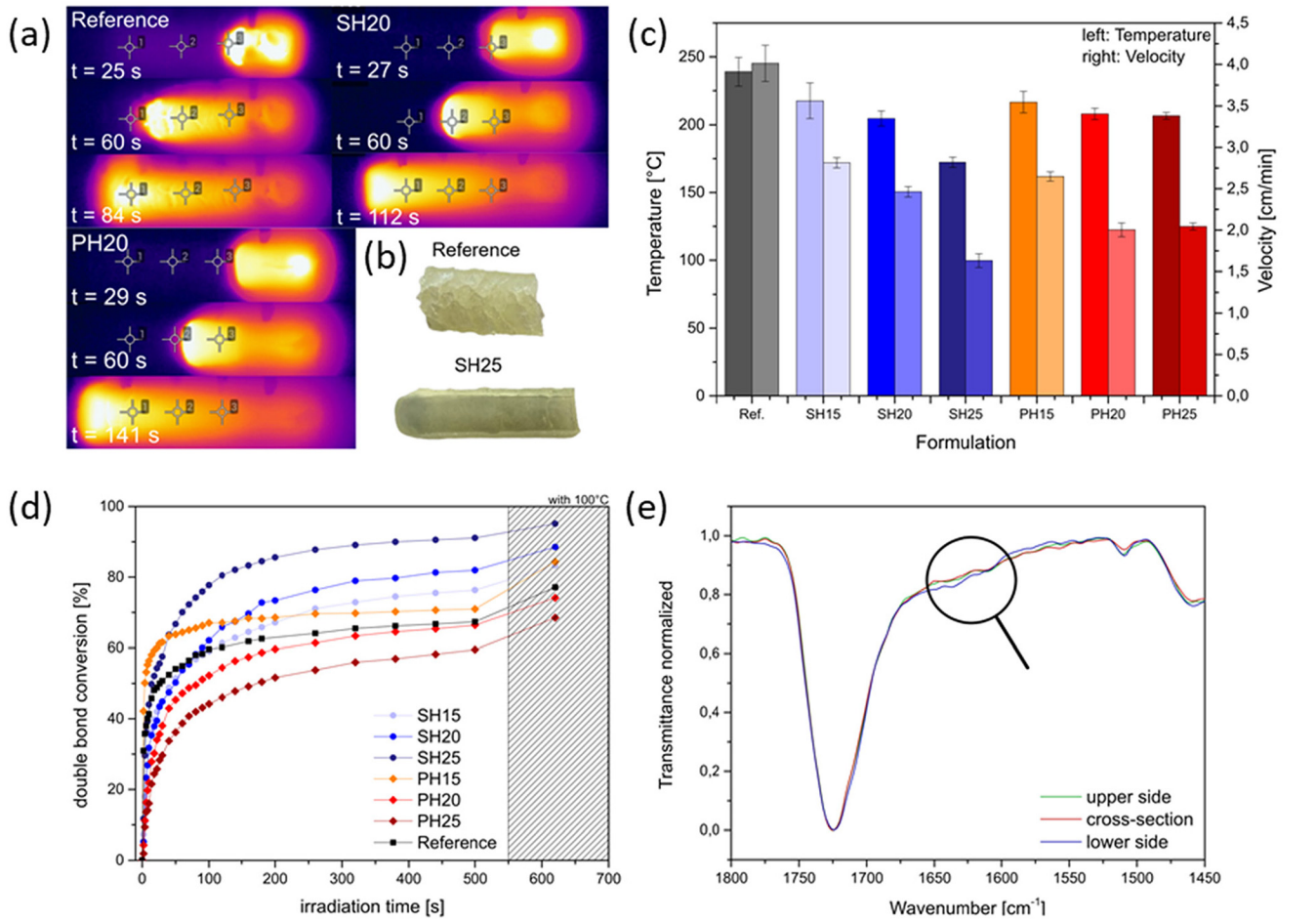

Fig. 2 Kinetics of reaction; (a) time-dependent thermograms of the frontal polymerization of the reference, SH20 and PH20 sample during front propagation; (b) image of the frontally cured reference and resin SH20 showing the difference in their surface quality; (c) frontal velocity and maximum temperature reached of the formulations under investigation; (d) carbon double bond conversions (decrease of the normalized C═C band between 1600 and 1650 cm^{-1}) of the samples under investigation *versus* irradiation time as measured by FTIR; (e) FTIR-spectra (wavelength range of the C═C absorption band has been magnified) of frontally polymerized resin SH20 taken from different areas of the test specimen.

for a thiol–acrylate system with a phosphate ester content of 4.7 mol%.[32] Furthermore, it has to be noted that by exceeding 20 mol% phosphate ester content, the pot-life of the resin is reduced since the thia-Michael side reaction is catalysed, which leads to premature curing of the resins. Moreover, only thin films were measured, and the kinetics obtained are only an approximation to a frontally polymerizing system, as this type of reaction will not propagate in such thin layers due to the high heat loss. To minimalize this error and to ensure mobility in the network over T_g, a final curing step above 100 °C was conducted. By increasing the temperature during irradiation, the final conversions could be increased by 4 to 13% in all systems depending on the T_g of the polymer network. However, frontal polymerization in bulk is expected to yield significantly higher conversions due to excessive heat generation. This can be seen in Fig. 2e, where a frontally polymerized SH20 sample was measured by ATR-FTIR spectroscopy. As can be seen, the acrylate peak (1600–1650 cm^{-1}) has completely disappeared through the sample's cross-section, indicating complete conversion.

2.2. Mechanical properties

Thermogravimetric analysis was carried out to determine the maximum operating temperature of the frontally cured photopolymers. All measured networks show similar behaviour with a 5% weight loss being achieved at temperatures between 280 and 290 °C (Fig. 3 ESI†). The varying thiol content does not affect the degradation temperature, whereas samples with varying phosphate content show a slight decrease in degradation temperature towards higher phosphate ester content. This can be explained by the flame-retardant properties of phosphate esters. A similar behaviour for a network containing the same phosphate ester molecule was reported in the literature.[33]

Dynamic mechanical analysis was carried out to determine the glass transition temperature (T_g) of the cured networks

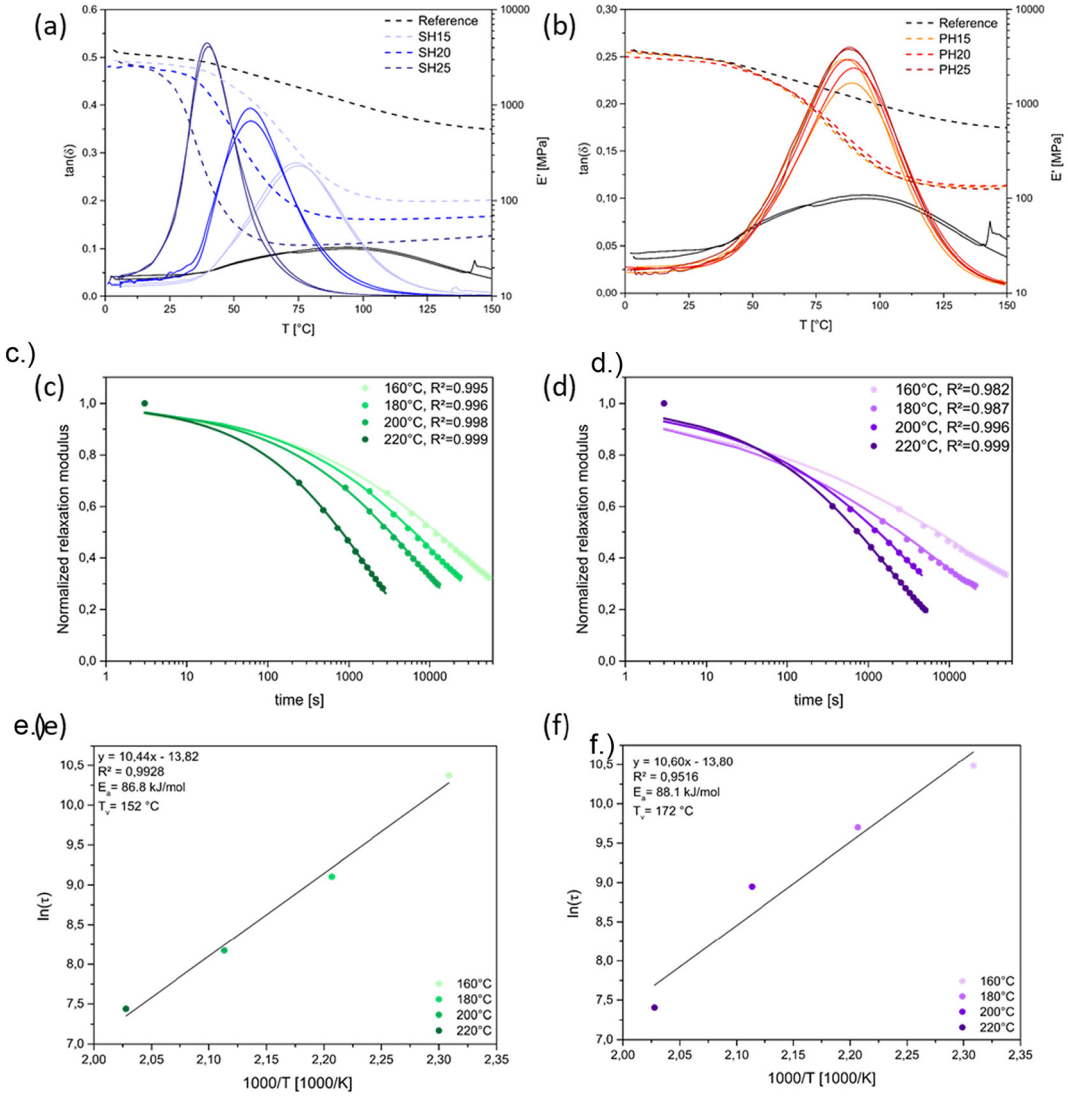

Fig. 3 Mechanical properties; DMA-curves of frontally cured samples (a) with varying thiol and (b) phosphate content; KWW modelled stress-relaxation measurements (c) of SH20 and (d) PH20 obtained at varying temperature; the Arrhenius plot of (e) SH20 and (f) PH20 with calculated T_v and E_a.

(Fig. 3a and b). For evaluation of the T_g, the peak of the loss factor was used. It was found that T_gs for resins with varying amounts (15 mol% to 25 mol%) of phosphate ester are in a similar range (88–89 °C). Moreover, the peak width for these formulations is comparable and ranged between 45 and 125 °C.

Whilst the content of methacrylated phosphate esters has a significant effect on the reactivity of the resin, the results reveal that its influence on the thermomechanical properties of frontally cured photopolymers is negligible.

In contrast, frontally cured resins with a higher amount of thiol feature a lower T_g. By varying the amount of thiol from 15 to 25 mol%, the T_g decreased from 75 °C (SH15) to 40 °C (SH25). Furthermore, the peak width decreased from 37–111 °C (SH15) to 24–65 °C (SH25). Compared to the peak width of the pure acrylate-based reference material (34–141 °C), it is confirmed that a higher amount of thiol increases the homogeneity of the network due to the simultaneous step-growth reaction mechanism. The lower T_g can be explained by a higher mobility of the networks, which is attributed to the higher flexibility of thioether bonds[29] and the decreased functionality of acrylates in thiol–ene step growth reactions. While acrylates have a functionality of two in homopolymerization, they possess only one single functionality in thiol–acrylate click reactions.

The storage modulus at room temperature (Fig. 3a and b) ranged between 2500–3500 MPa, followed a similar trend to the T_g values. By varying the phosphate ester content, no significant change in the storage modulus at room temperature was observed. In contrast, the acrylate-based photopolymer (reference) is significantly more rigid, even at elevated temperatures. The decrease in storage modulus at elevated tempera-

ture for formulations with varying phosphate ester contents seems to be in accordance with the tan(δ) measured as E' lies between 125 and 132 MPa. However, at elevated temperature, a significant variation in the decrease of storage modulus for formulations with increasing thiol content can be observed, as it ranges between 100 MPa for SH15 and 42 MPa for SH25. Thus, resins containing higher amounts of thiol are softer and are expected to be reprocessed more easily due to their higher mobility.

In addition to the DMA-measurements, swelling tests were conducted. The degree of swelling decreases with increasing phosphate ester content from 114.3 ± 3.5% to 109.8 ± 1.8% (Fig. 4 ESI; Table 5 ESI†), which is in good agreement with the FTIR data. In contrast, a higher degree of swelling is measured with an increasing amount of thiol. In particular, it increased from 117.5 ± 0.3% to 210.7 ± 3.1 for SH15 and SH25, respectively. This is due to the lower degree of crosslinking obtained by thiol–ene chemistry compared to acrylate homopolymerization.

The high gel contents in general can be explained by the high conversion reached by frontal polymerization. In addition, similarly high gel contents have been reported in the literature for the better investigated frontal polymerization of epoxies.[34] Consequently, it can be deduced that material properties such as T_g, softness and cross-linking density can be fine-tuned by varying the thiol content whilst the amount of catalyst plays a minor role.

To characterize the dynamic properties of the developed systems, stress-relaxation measurements were carried out at 200 °C. Prior to these measurements, an amplitude sweep experiment was carried out for SH20 as well as for PH20 at 200 °C to determine a suited strain within the viscoelastic domain (Fig. 5 ESI†). Subsequently a strain of 1% was applied. The resulting curves are shown in Fig. 6 ESI and 7 ESI.† The characteristic relaxation times (τ) were acquired according to the Maxwell model at 1/e. This model was chosen as it is the best suited for describing viscoelastic materials.[35] It was found that increasing either thiol or phosphate ester content leads to less time required to relax 63% of initial stress. In particular, it was observed that the relaxation times decrease from 35 808 s (reference) to 9021 s (SH15) and 6225 s (SH25) when increasing the thiol content from 0 to 15 and 25 mol%, respectively (Table 6 ESI†). As the number of thioether bonds increases the flexibility and lowers the T_g of the networks, the faster relaxation kinetics can be mainly explained by the higher network mobility.

In contrast, the phosphate ester content did not considerably affect the thermomechanical properties (and thus the mobility of the network). However, it served as a transesterification catalyst and significantly reduced the relaxation times from 6684 s (PH15) to 2391 s (PH25) by increasing its concentration from 15 to 25 mol%.[27] The results are in good agreement with the literature that reports accelerated bond exchange rates with increasing catalyst content.

Resins SH20 and PH20 were studied in more detail in order to monitor their relaxation at temperatures varying from 160 °C to 220 °C (Fig. 3c and d, and non-normalized curves are shown in Fig. 8 ESI†). For these measurements, the data obtained were modelled with the Kohlrausch–Williams–Watts-function (KWW) (eqn (1) ESI†), since it is best suited to describe non-ideal stress relaxation behaviour.[36] These formulations were chosen, as thiol–acrylate resins with 25 mol% thiol or phosphate were prone to dark reactions and became unstable during storage. In general, the stress–relaxation process is accelerated toward higher temperatures as the phosphate ester-catalyzed dynamic exchange proceeds more rapidly. In respect thereof, a temperature dependence of the characteristic relaxation time acquired with the KWW model (τ_{KWW}) according to the Arrhenius relationship (eqn (2) ESI†) represents one of the key characteristics of dynamic polymer networks undergoing an associative exchange mechanism. Both networks showed a linear dependency of τ_{KWW} on $(1/T)$ in a semilogarithmic scale and thus an Arrhenius-type behaviour is confirmed (Fig. 3e and f).

In addition, the activation energy (E_a) was calculated from the equation of the linear fit by multiplying the slope by the ideal gas constant R. The two calculated activation energies, displayed in Fig. 3e and f, are comparably high and lie within the range of 29–163 kJ mol^{-1} given in the literature for transesterification.[37]

Additionally, the topology freezing temperature (T_v) was calculated from the linear fit in combination with the DMA results. For this calculation, it was assumed that the T_v occurs at a viscosity of 10^{12} Pa s, as suggested in the literature.[29] Interestingly, frontally cured SH20 and PH20 yield T_v values of 152 °C and 172 °C, respectively, which correspond well to their difference in T_gs (56 °C for SH20 and 89 °C for PH20) (Fig. 3e and f). This trend is attributed to the increased mobility in the SH20 network (due to an higher amount of thiol), which has a positive effect on the stress relaxation behaviour by promoting it. The increased concentration of the catalyst in the PH20 network should also lead to shorter relaxation times. However, by comparing the performance of the two networks under investigation, it can be assumed that the influence of network mobility on T_v is more pronounced than the catalyst concentration (in the investigated concentration range).

2.3. Reshaping and recycling

To exploit the dynamic network properties, confirmed by stress-relaxation experiments, a reshaping experiment of frontally cured resin SH20 was performed (Fig. 4a). The test specimen was programmed at two different temperatures: first at 100 °C ($T > T_g$) and in the second step at 180 °C ($T > T_v$) as described in the ESI.† The shape recovery was tested by heating up the sample above T_g and the material relaxed back into its first programmed shape. Due to the thermo-activated topological rearrangements, the network was able to be kept in shape, which has been programmed at 180 °C. The colour change observed in several types of networks is most likely from oxidation. We assume that in the current networks under investigation it is amplified due to the incorporated phosphate ester, as phosphorus is known for its oxophilicity, especially at elevated temperatures.[38]

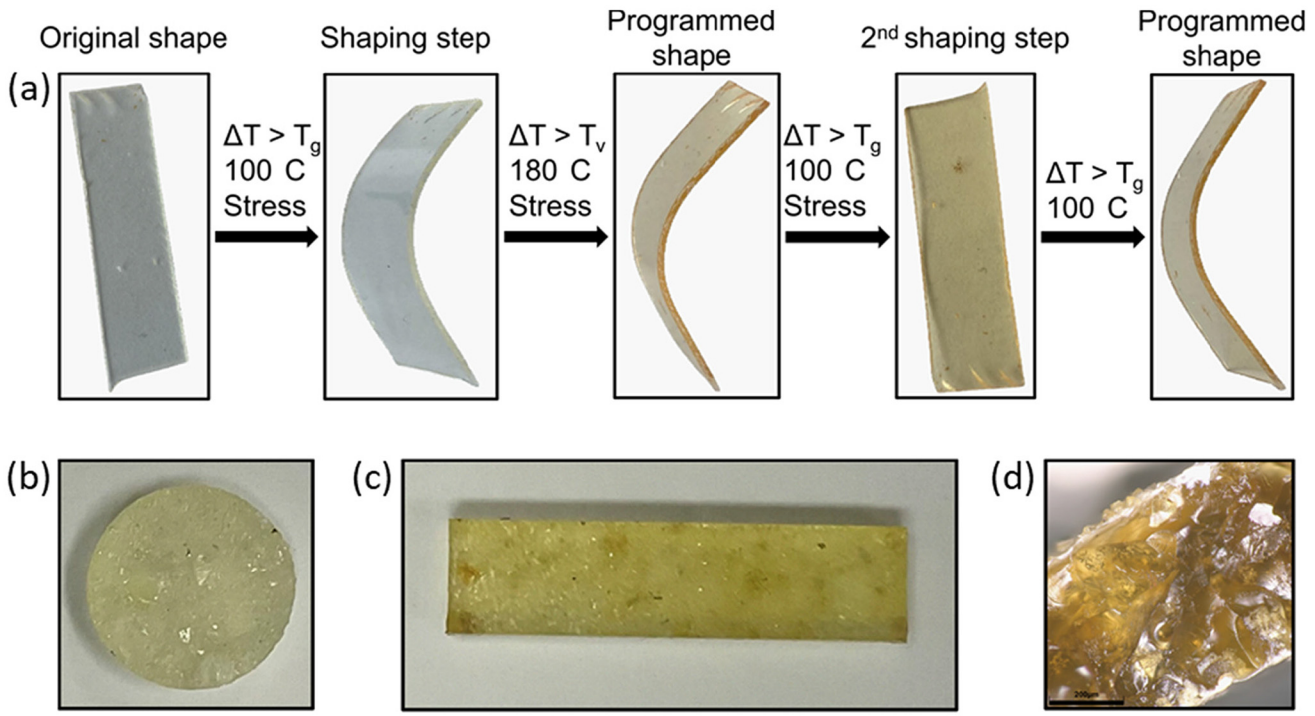

Fig. 4 (a) Reshaping of frontally cured SH20 over T_g and reprogramming over T_v and subsequent 2nd reshaping over T_g; (b) 8 mm ∅ sample made with the VCM device at 170 °C for 1 h; (c) sample made with the VCM device at 210 °C for 1 h; (d) microscopy cross-section of the pressed sample.

Furthermore, to underline the advantageous properties of dynamic networks, reprocessing experiments were conducted. Therefore, a frontally polymerized cylinder was cryo-ball milled and subsequently reprocessed using a vacuum compression moulding (VCM) device provided by the company Meltprep. As the VCM device offers several moulds, samples with different geometries were produced (Fig. 4b and c). The main limitation of the VCM device is the maximum pressure achievable. The

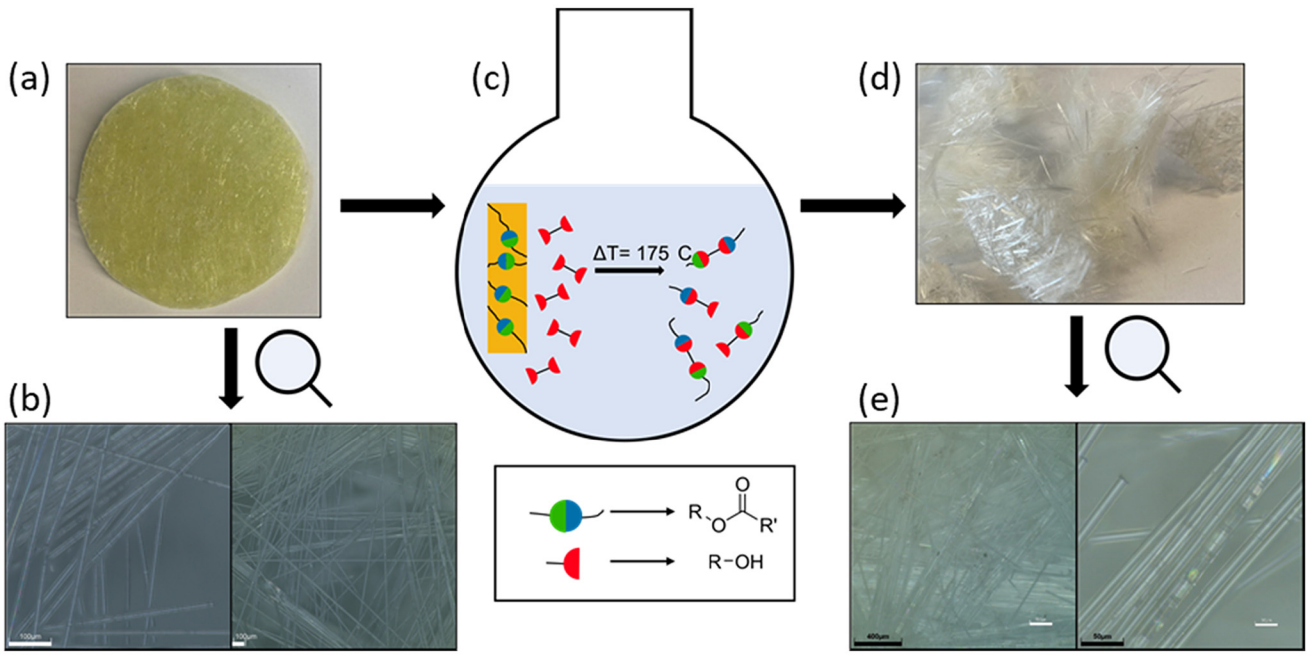

Fig. 5 (a) Frontally cured composite of glass fibres and SH20; (b) microscopy images of the virgin glass fibres at 140-fold magnification and at 500-fold magnification; (c) scheme of depolymerization in ethylene glycol; (d) recovered glass fibres; (e) microscopy images of recovered glass fibres at 140-fold magnification and at 500-fold magnification.

pressure depends on the quality of the vacuum, meaning that higher pressure can be achieved with smaller sample chambers. Since the maximum pressure is limited by the sample geometry, vacuum compression moulding at lower pressures works better with softer materials than with stiff ones. This can especially be observed in Fig. 7 ESI,† which shows various samples produced with the VCM device. It can be seen that reprocessing of SH20 samples (see Fig. 9 ESI†) resulted in good quality, while PH20 samples could not be reprocessed sufficiently. As SH20 and PH20 networks showed similar stress relaxation kinetics, the results suggest that the glass transition temperature and network mobility are mainly affecting the reprocessing properties of the frontally cured photopolymers. Thus, further experiments were carried out with SH20.

By analysing the cross-section of the reprocessed SH20 sample, only minor defects at the edges of the object were observed (Fig. 4d). The recovery of the material properties was tested with Shore-D-hardness. While the virgin sample reached a Shore-D hardness of 82.8 ± 1.5, the reprocessed sample featured a hardness of 73.6 ± 3.3, corresponding to 88.9% of the original one. As the hardness of the material depends on the crosslinking density, it can be used as an initial test to confirm the success of the reprocessing.[39]

To demonstrate the possibility of the developed networks towards the chemical recycling of technically relevant composites, frontally cured composites containing 5 wt% of glass fibres were produced. By exploiting transesterification reactions between the network and a solvent at elevated temperatures, the sample was emerged in ethylene glycol, which directly attacks the ester moieties, leading to alcoholysis.[40] It should be noted that the composite was frontally polymerized by using a soldering iron as the thermal trigger. The reaction could not be started by light due to scattering of the glass fibres, which led to conventional photopolymerization. Subsequently, the resulting sample was cut into smaller pieces and emerged in ethylene glycol at 200 °C for 72 h. The glass fibres were recovered and washed using ethanol. A comparison of the virgin and recovered glass fibres was done with light microscopy (Fig. 5). Here, it can be seen that the recovered fibers did not contain any polymer residues on their surface. This is an important aspect for manufacturing and recycling of dynamic polymer composites in future applications. Furthermore, the resulting polymer matrix residue might also be used for further applications. This could be achieved either by a polycondensation reaction with an anhydride, or by crosslinking with an epoxide, since –OH groups are abundant in the resulting oligomeric mixture.

3. Conclusion

This study shows that frontal polymerization is a very well suited and energy-efficient method for the production of covalent adaptable networks. Using this technique, high monomer conversions can be achieved as well as fast curing. Moreover, we have demonstrated that network properties can be fine-tuned by varying the thiol amount used. The resulting networks showed rapid relaxation at 220 °C and linear dependency in an Arrhenius-like manner. To underline the versatility of the developed material, reshaping as well as reprocessing were successfully demonstrated, reaching 88.9% of the original Shore-D hardness. Moreover, it is possible to recover fibers from a frontally cured polymer composite by dissolution of the covalent adaptable network in a suitable solvent. To conclude, this study demonstrates the combination of dynamic networks with frontal polymerization, and thus merging their energy efficiency and reworking properties. Hence, this investigation provides a new perspective on the efficient production of circular thermosets and their composites.

Data availability

The data supporting this article have been included as part of the ESI.†

Conflicts of interest

The authors declare no conflict of interest.

Acknowledgements

The research work was performed within the COMET-project "Photostructurable Encapsulation Molds and Magnetic Composites" (project-no.: VII-S2) at the Polymer Competence Center Leoben GmbH (PCCL, Austria) within the framework of the COMET-program of the Federal Ministry for Climate Action, Environment, Energy, Mobility, Innovation and Technology and the Federal Ministry for Digital and Economic Affairs with contributions by the Graz University of Technology. The PCCL is funded by the Austrian Governments and the State Governments of Styria, Lower Austria and Upper Austria. The authors thank Andreas Bramböck (MeltPrep GmbH) and Belma Bacic (MeltPrep GmbH) for supplying the VCM device and producing additional samples. Moreover, the authors thank Thomas Rath, Marco Sigl as well as Melissa Egger from the Institute of Technology and Chemistry of Materials from TU Graz and Sebastian Maar from PCCL for conducting the DMA measurements.

References

1 Q. Li, H.-X. Shen, C. Liu, C.-F. Wang, L. Zhu and S. Chen, *Prog. Polym. Sci.*, 2022, **127**, 101514.
2 J. A. Pojman, *J. Am. Chem. Soc.*, 1991, 6284.
3 D. Bomze, P. Knaack, T. Koch, H. Jin and R. Liska, *J. Polym. Sci., Part A:Polym. Chem.*, 2016, **54**, 3751.
4 M. S. Malik, M. Wolfahrt and S. Schlögl, *RSC Adv.*, 2023, **13**, 28993.

5 S. Sutthasupa, M. Shiotsuki and F. Sanda, *Polym. J.*, 2010, **42**, 905.
6 I. D. Robertson, M. Yourdkhani, P. J. Centellas, J. E. Aw, D. G. Ivanoff, E. Goli, E. M. Lloyd, L. M. Dean, N. R. Sottos, P. H. Geubelle, *et al.*, *Nature*, 2018, **557**, 223.
7 J. Bachmann, C. Hidalgo and S. Bricout, *Sci. China: Technol. Sci.*, 2017, **60**, 1301.
8 I. D. Robertson, M. Yourdkhani, P. J. Centellas, J. E. Aw, D. G. Ivanoff, E. Goli, E. M. Lloyd, L. M. Dean, N. R. Sottos, P. H. Geubelle, *et al.*, *Nature*, 2018, **557**, 223.
9 P. J. Centellas, M. Yourdkhani, S. Vyas, B. Koohbor, P. H. Geubelle and N. R. Sottos, *Composites, Part A*, 2022, **158**, 106931.
10 P. Garra, C. Dietlin, F. Morlet-Savary, F. Dumur, D. Gigmes, J.-P. Fouassier and J. Lalevée, *Polym. Chem.*, 2017, **8**, 7088.
11 R. Tiani, J. A. Pojman and L. Rongy, *J. Phys. Chem. B*, 2022, **126**, 3607.
12 D. I. Fortenberry and J. A. Pojman, *J. Polym. Sci., Part A: Polym. Chem.*, 2000, **38**, 1129.
13 B. A. Suslick, J. Hemmer, B. R. Groce, K. J. Stawiasz, P. H. Geubelle, G. Malucelli, A. Mariani, J. S. Moore, J. A. Pojman and N. R. Sottos, *Chem. Rev.*, 2023, **123**, 3237.
14 E. Morici and N. T. Dintcheva, *Polymers*, 2022, **14**, 4153.
15 W. Post, A. Susa, R. Blaauw, K. Molenveld and R. J. I. Knoop, *Polym. Rev.*, 2020, **60**, 359.
16 S. Leszczyński and B. Brzychczyk, *Pol. J. Chem. Technol.*, 2007, **9**, 122.
17 H. Zhang, J. Cui, G. Hu and B. Zhang, *Int. J. Smart Nano Mater.*, 2022, **13**, 367.
18 C. J. Kloxin, T. F. Scott, B. J. Adzima and C. N. Bowman, *Macromolecules*, 2010, **43**, 2643.
19 U. Shaukat, A. Thalhamer, E. Rossegger and S. Schlögl, *Addit. Manuf.*, 2024, **79**, 103930.
20 J. L. Self, N. D. Dolinski, M. S. Zayas, J. Read de Alaniz and C. M. Bates, *ACS Macro Lett.*, 2018, **7**, 817.
21 S. Bhusal, C. Oh, Y. Kang, V. Varshney, Y. Ren, D. Nepal, A. Roy and G. Kedziora, *J. Phys. Chem. B*, 2021, **125**, 2411.
22 W. Alabiso and S. Schlögl, *Polymers*, 2020, **12**, 1660.
23 G. Rizzo, L. Saitta, S. Dattilo, C. Tosto, E. Pergolizzi, A. Ivankovic and G. Cicala, *ACS Appl. Polym. Mater.*, 2023, **5**, 8326.
24 A. Gablier, M. O. Saed and E. M. Terentjev, *Soft Matter*, 2020, **16**, 5195.
25 D. Reisinger, A. Hellmayr, M. Paris, M. Haas, T. Griesser and S. Schlögl, *Polym. Chem.*, 2023, **14**, 3082.
26 E. Rossegger, R. Höller, D. Reisinger, J. Strasser, M. Fleisch, T. Griesser and S. Schlögl, *Polym. Chem.*, 2021, **12**, 639.
27 E. Rossegger, R. Höller, D. Reisinger, M. Fleisch, J. Strasser, V. Wieser, T. Griesser and S. Schlögl, *Polymer*, 2021, **221**, 123631.
28 J. A. Pojman, B. Varisli, A. Perryman, C. Edwards and C. Hoyle, *Macromolecules*, 2004, **37**, 691.
29 W. Alabiso, T. M. Hron, D. Reisinger, D. Bautista-Anguís and S. Schlögl, *Polym. Chem.*, 2021, **12**, 5704.
30 C. E. Hoyle and C. N. Bowman, *Angew. Chem., Int. Ed.*, 2010, **49**, 1540.
31 A. P. Fugolin, A. Dobson, W. Mbiya, O. Navarro, J. L. Ferracane and C. S. Pfeifer, *Dent. Mater.*, 2019, **35**, 686.
32 K. Moazzen, E. Rossegger, W. Alabiso, U. Shaukat and S. Schlögl, *Macro Chem. Phys.*, 2021, **222**, 2100072.
33 X. Feng and G. Li, *ACS Appl. Mater. Interfaces*, 2020, **12**, 57486.
34 J. Zhou, S. Jia, W. Fu, Z. Liu and Z. Tan, *Mater. Lett.*, 2016, **176**, 228.
35 F. Meng, M. O. Saed and E. M. Terentjev, *Nat. Commun.*, 2022, **13**, 5753.
36 F. Cuminet, D. Berne, S. Lemouzy, É. Dantras, C. Joly-Duhamel, S. Caillol, É. Leclerc and V. Ladmiral, *Polym. Chem.*, 2022, **13**, 2651.
37 F. Cuminet, S. Caillol, É. Dantras, É. Leclerc and V. Ladmiral, *Macromolecules*, 2021, **54**, 3927.
38 L. Cho and E. E. Klaus, *ASLE Trans.*, 1981, **24**, 119.
39 N. Lorwanishpaisarn, N. Srikhao, K. Jetsrisuparb, J. T. N. Knijnenburg, S. Theerakulpisut, M. Okhawilai and P. Kasemsiri, *J. Polym. Environ.*, 2022, **30**, 472.
40 D. Santiago, D. Guzmán, J. Padilla, P. Verdugo, S. de La Flor and À. Serra, *ACS Appl. Polym. Mater.*, 2023, **5**, 2006.